Available online at www.sciencedirect.com

jmr&t Journal of Materials Research and Technology

journal homepage: www.elsevier.com/locate/jmrt

Original Article

Effect of post-deformation annealing on the microstructure and mechanical behavior of an Fe–Ni–Mn steel processed by high-pressure torsion

Hamidreza Koohdar [a,*], *Mahmoud Nili-Ahmadabadi* [b,c], *Faezeh Javadzadeh Kalahroudi* [b], *Hamid Reza Jafarian* [a], *Terence G. Langdon* [d]

[a] *School of Metallurgy and Materials Engineering, Iran University of Science and Technology (IUST), Narmak, Tehran, Iran*

[b] *School of Metallurgy and Materials Engineering, University of Tehran, P.O. Box 14395-731, Tehran, Iran*

[c] *Center of Excellence for High Performance Materials, School of Metallurgy and Materials Engineering, University of Tehran, Tehran, Iran*

[d] *Materials Research Group, Department of Mechanical Engineering, University of Southampton, Southampton SO17 1BJ, UK*

ARTICLE INFO

Article history:
Received 4 May 2021
Accepted 29 August 2021

Keywords:
Fe-Ni-Mn steel
High-pressure torsion
Post-deformation annealing
Mechanical behavior
Microstructural evolution

ABSTRACT

Research was conducted to investigate the effects of high-pressure torsion (HPT) and post-deformation annealing (PDA) on the microstructure evolution and mechanical behavior of an Fe-9.6Ni-7.1Mn (at.%) steel with an initial lath martensitic microstructure. The experimental results showed that HPT processing led to the formation of an ultrafine grain martensitic microstructure accompanied by small amounts of strain-induced austenite. Phase analysis and microstructural examination confirmed that during PDA at 600 °C a large fraction of fine and coaxial austenite grains was introduced in the microstructure by diffusionless shear mechanism whereas its volume fraction at ambient temperature was drastically decreased by increasing the annealing time. Also, the grain size was reduced from a value of about 5.2 μm in the solution-treated specimen to ultrafine values of about 570 and 280 nm for the martensite and austenitic phases, respectively, after PDA for 7.2 ks. PDA yielded an outstandingly good combination of an ultimate tensile strength (~1340 MPa) and fracture strain (~11.9%) in comparison to the solution-annealed condition which can be attributed to the finer grain size and the presence of shear-formed austenite in the microstructure. In addition, the fracture mode changed from a fully ductile nature in the solution-treated specimen to a combination of ductile and brittle nature after applying the HPT and then returned again to a ductile behavior after PDA.

* Corresponding author.
E-mail address: hkoohdar@iust.ac.ir (H. Koohdar).

https://doi.org/10.1016/j.jmrt.2021.08.135

1. Introduction

Fe-9.6Ni-7.1Mn (at.%) alloy having the lath martensite matrix with a high density of dislocations is categorized as a high strength steel. This alloy has a ductile nature in the solution-treated condition and is susceptible to age hardening through the θ-NiMn precipitates formation. However, it suffers from a severe embrittlement along prior austenite grain boundaries after aging [1–3]. Recently, various severe plastic deformation (SPD) methods such as severe cold rolling [4–7], equal-channel angular pressing (ECAP) [8] and high-pressure torsion (HPT) [9–11] have been applied to the present alloy in order to improve the mechanical properties. Under SPD processing, in addition to the grain refinement, the strain-induced austenite by a diffusionless shear mechanism can be partially formed in the martensitic microstructure which improves the mechanical properties [4–6,9]. The other promising way to achieve strengthened and toughened Fe-9.6Ni-7.1Mn martensitic steel is to use a suitable annealing treatment in the two phase (ferrite + austenite) region which can stabilize the diffusional or diffusionless reversed austenite in martensite microstructure with appropriate grain size and morphology [12–17].

Processing by SPD can easily introduce high values of plastic strain even in materials having limited ductility [18,19]. Since under HPT processing, a large compressive hydrostatic stress is introduced therefore, it is the most effective method for processing difficult-to-work alloys compared to the others SPD techniques [20,21]. In this process, a thin disk-shaped specimen is compressed between two rigid anvils and subjected to torsional shear straining. As HPT processing has considerable characteristics such as significant grain refinement [22], a high density of lattice defects [23–25], high strength and hardness [26], superplastic properties [27] and reasonable thermal stability [28,29] therefore, it has attracted many researchers in two recent decades.

Using SPD processing leads to a temperature decrease in re-crystallization and austenitization during subsequent annealing [28]. Additionally, an annealing treatment after SPD processing may produce small austenite grains in the α′-martensitic microstructure such that a mixture of high strength and fine ductility becomes feasible [29,30]. A combination of HPT processing and subsequent annealing has a great impact in introducing a newly formed austenite with a smaller grain size even at higher temperatures by comparison with annealing without pre-deformation [31]. It was reported that, following a high temperature annealing treatment of the HPT-processed austenitic stainless steel, a reverse transformation of α′-martensite to the γ-austenite (reverse transformation) yielded a fully austenitic microstructure with a small grain size of around 200 nm which gave remarkably high strength with a good ductility compared with the initial steel [32]. During annealing, the reverse transformation can take place by two competing mechanisms consisting of diffusional and diffusionless shear mechanisms. The predominant mechanism of the reverse transformation is sensitive to the chemical composition of the alloy and the fundamental parameters of the heat treatment such as the annealing temperature and the imposed time [33–37].

Recently, the effect of HPT processing with different numbers of turns on the microstructure and mechanical behavior of an Fe-9.6Ni-7.1Mn (at.%) steel in different conditions was studied [9,10]. The results demonstrated that the initial microstructure, grain size and constituent phases have crucial impact on the mechanical behaviors of the alloy. In fact, a severely deformed structure would promote phase transformations, ultrafine grain development and also supply a high density of nucleation sites with faster diffusion tracks. Accordingly, the present study was conducted to examine the effect of prior HPT processing on the reversed austenite formation in the microstructure of Fe-9.6Ni-7.1Mn (at.%) lath martensitic steel during post-deformation annealing (PDA) in the dual phase (ferrite + austenite) region. Additionally, the effects of prior HPT processing and PDA on the microstructure and mechanical behavior of the steel were studied.

2. Experimental procedures

An ingot of the Fe-9.6Ni-7.1Mn (at.%) alloy was provided using a non-consumable vacuum arc re-melting furnace and then forged through 50% reduction in thickness at 1200 °C in order to break the dendritic structure. The forged ingot was homogenized at 1100 °C for 172.8 ks in an atmosphere controlled tube furnace and then solution treated at 900 °C for 3.6 ks followed by quenching in cold water in order to achieve a fully lath α′-martensitic microstructure. The nominal composition of the prepared ingot is given in Table 1.

For applying HPT, some disk-shape samples with a diameter of 10 mm and a thickness of 0.8 mm were cut from the solution-treated (ST) specimen and then processed by HPT for 20 turns at ambient temperature under quasi-constrained conditions [38] in 6.0 GPa pressure and rotation rate of 1 rpm.

Post-deformation annealing (PDA) was carried out on the HPT-processed samples in a salt bath at 600 °C in the two phase (ferrite + austenite) region for 0.04, 0.48, 1.8 and 7.2 ks annealing times followed by cooling to room temperature. According to an earlier report [13], the austenite start (A_s) and austenite finish (A_f) temperatures were measured at about 570 and 640 °C, respectively, and therefore, the above mentioned temperature was in the two phase (ferrite + austenite) region. A schematic illustration of the thermo-mechanical process including HPT and PDA is presented in Fig. 1.

Table 1 – Nominal composition of the prepared ingot.

Element	Fe	Ni	Mn	P	S	C	N	Al
At.%	Bal.	9.62	7.11	0.008	0.006	0.004	0.003	0.003

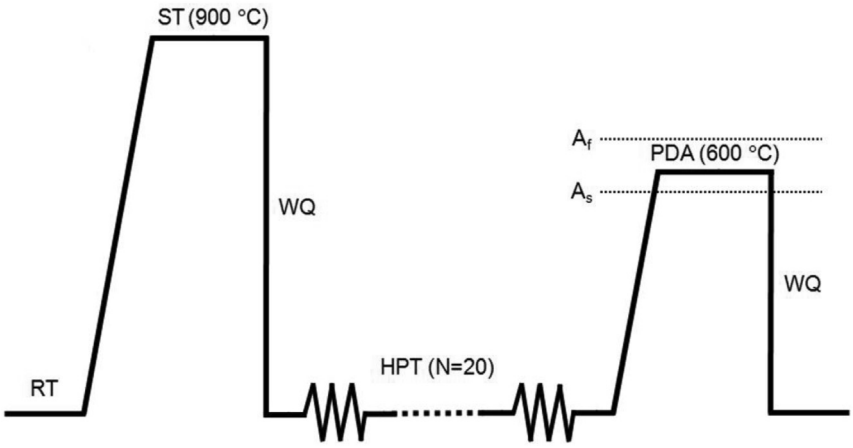

Fig. 1 – Schematic representation of the thermo-mechanical process consisting of HPT and PDA.

Phase analysis was conducted by X-ray diffraction (XRD) method with Cu-K_α radiation. It was performed using a step scanning rate of 0.01° per 1.8 s over a range of 2θ between 40 and 100°. Also, the microstructure of the specimens was characterized using field emission scanning electron microscopy (FE-SEM) coupled with an electron backscatter diffraction (EBSD) detector operating at 15 kV. In this case, for microstructural characterization, a section of the specimens was mechanically polished followed by electrolytically etched in a chemical solution of 900 ml CH_3COOH and 100 ml $HClO_4$ at a temperature of 11 °C and a voltage of 25 V. The EBSD analysis was carried out by a step size of 20 nm and evaluated by using TSL-OIM software.

Micro-hardness measurements were taken on the polished surfaces using a Vickers micro-hardness tester with a load of 200 gf and dwell times of 10 s. In addition, tensile tests at ambient temperature were conducted on the miniature tensile specimens with gauge dimensions of 1.8 × 0.8 × 0.5 mm^3 using a SANTAM testing machine with an initial strain rate of 6.0×10^{-4} s^{-1}. The fracture surfaces were also characterized by FE-SEM.

3. Results

3.1. Microstructure and phase evolution

Figure 2 shows the XRD patterns of the ST specimen, the HPT-processed sample and the PDA-processed specimens for different annealing times as pointed on the right. For the ST and the HPT-processed specimens, only the peaks corresponding to α′-martensite were observed and there was no trace of a γ-austenite peak. However, in the PDA-processed specimens, beside the α′-martensite peaks, five additional peaks were also detected which corresponded to the various planes of the austenite phase.

The volume fractions of the retained austenite at ambient temperature after PDA for various annealing times were obtained by XRD as indicated in Fig. 3. It is observed that the retained austenite value in the PDA-processed specimen for 0.04 ks is about 58% which decreases by increasing the

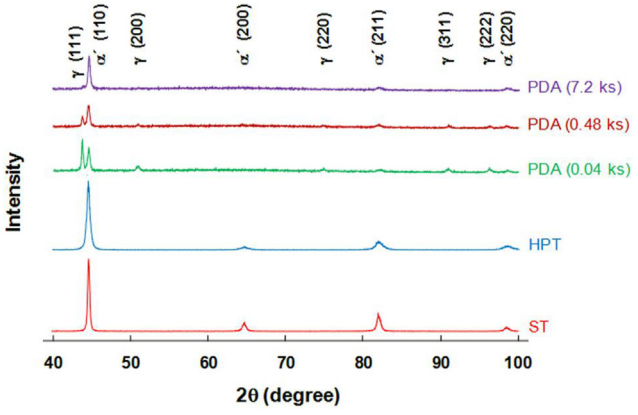

Fig. 2 – XRD patterns of the ST specimen, the HPT-processed sample, and the PDA-processed specimens for indicated times.

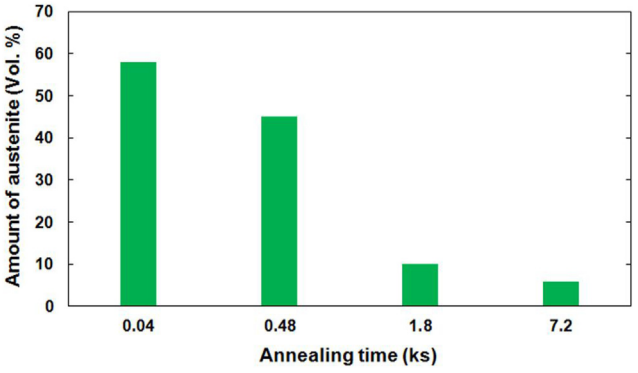

Fig. 3 – Amount of the retained austenite at ambient temperature after PDA for different annealing times obtained from the XRD results.

annealing time such that only about 6% of the austenite is stable at room temperature after PDA for 7.2 ks.

The grain boundary phase maps obtained from EBSD analysis for (a) the ST specimen, (b) the HPT-processed sample and (c-f) the PDA-processed specimens for different annealing

times are presented in Fig. 4 so that the pink and green colors indicate the α′-martensite and austenite, respectively. The superimposed red and black lines are, respectively, low-angle grain boundaries (LAGBs: <15 deg) and high-angle grain boundaries (HAGBs: θ ≥ 15 deg). Based on Fig. 4(a), the microstructure of the ST specimen consisted of typical lath α′-martensite including packet and block as a substructure of lath martensite with a high fraction of LAGBs. By contrast, the microstructure of the HPT-processed specimen in Fig. 4(b) shows a mixture of equiaxed and elongated martensitic ultrafine grains accompanied by small fraction of fine-grained austenite. The observed austenite is due to the strain-induced reverse transformation during the HPT processing. This consequence is not consistent with the results of XRD in Fig. 2. After PDA of the HPT-processed specimen for 0.04 ks as illustrated in Fig. 4(c), a large fraction of the fine and coaxial austenite grains was nucleated in the deformed martensitic microstructure due to the occurrence of the reverse transformation such that its volume fraction drastically decreased by increasing the annealing times (Fig. 4(d)–(f)). This indicates that, by increasing the annealing time, a significant amount of the reversed austenite re-transformed to the new martensite under subsequent cooling to ambient temperature. Moreover, it appears that the volume fraction of LAGBs significantly decreased in the initial times of the PDA due to the reduction of dislocations density through the occurrence of a recovery process and then increased in further annealing times as a result of a re-transformation of austenite to the new martensite with a high amount of dislocations. The volume fractions of LAGBs and HAGBs in different conditions as measured by EBSD are indicated in Fig. 5.

The average grain sizes of the different phases achieved from the EBSD maps in the ST specimen, the HPT-processed sample and the PDA-processed specimens for different

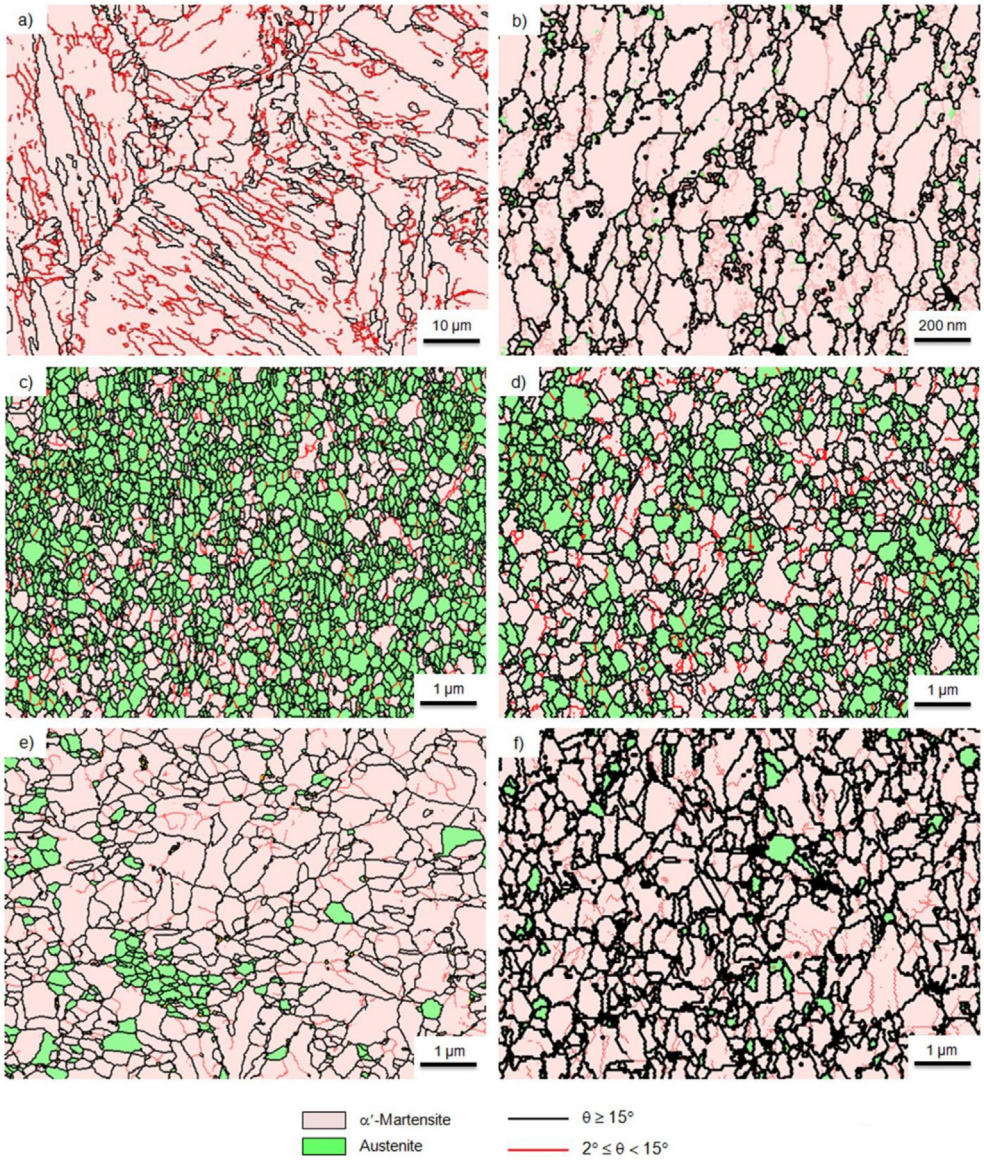

Fig. 4 – Grain boundary and phase maps achieved from the EBSD analysis for (a) the ST specimen, (b) the HPT-processed sample, and the PDA-processed specimens for (c) 0.04 ks, (d) 0.48 ks, (e) 1.8 ks and (f) 7.2 ks.

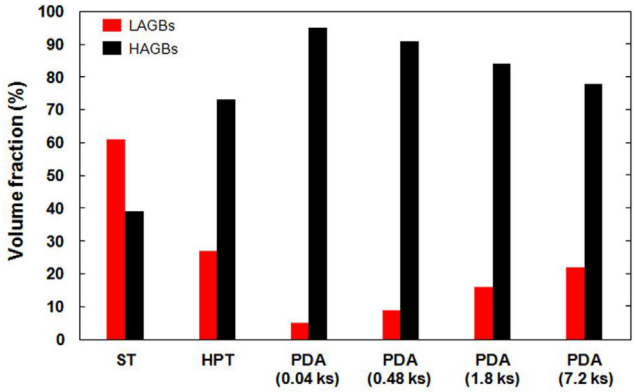

Fig. 5 – The volume fractions of LAGBs and HAGBs resulted from the EBSD analysis in the ST specimen, the HPT-processed sample, and the PDA-processed specimens for various annealing times.

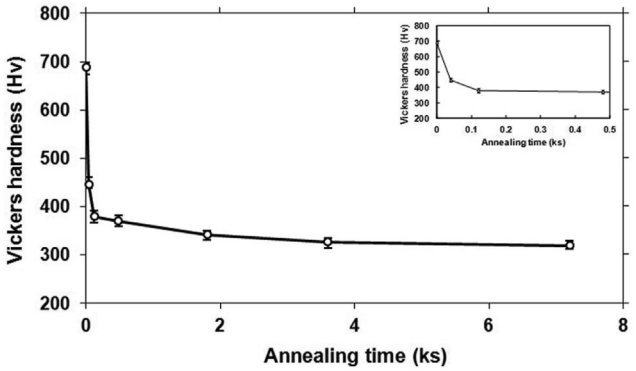

Fig. 6 – Vickers micro-hardness values for the HPT-processed sample and the PDA-processed specimens for various annealing times. The inset indicates the micro-hardness values in the initial steps of PDA.

annealing times are indicated in Table 2. As expected, the average grain size was reduced from about 5.2 μm in the ST specimen to around 185 nm for the martensite and around 28 nm for the austenite in the HPT-processed sample. The reported average grain size of martensite in the ST specimen is a mean of the blocks size. It is difficult to achieve smaller martensitic grains under HPT processing compared to austenitic ones because the martensite has a high density of dislocations which makes it difficult to recognize dislocation generation as the major source of grain subdivision. In the PDA-processed specimen for 0.04 ks, the average grain sizes of the martensite and retained austenite were about 195 and 180 nm, respectively. By increasing the annealing time, the average grain sizes of the two phases increased but not at the same rate so that after PDA for 7.2 ks the average grain sizes of martensite and retained austenite were measured as about 570 and 280 nm, respectively.

3.2. *Mechanical properties*

Figure 6 shows the results for the Vickers micro-hardness, Hv, for the HPT-processed sample and the PDA-processed specimens for different annealing times where each experimental result relates to the average of five discrete measurements. The micro-hardness of the HPT-processed sample was about 690 Hv which decreased to around 445 Hv after PDA for only 0.04 ks. A next increase in the annealing time led to a slow decline in the micro-hardness such that it eventually reached less than 320 Hv. As reported earlier [13], the micro-hardness of the ST specimen was measured at about 275 Hv which is lower than the micro-hardness of the PDA-processed specimens.

Figure 7 shows the representative plots of engineering stress against engineering strain at ambient temperature for the initial ST specimen, the HPT-processed sample and the PDA-processed specimens for 0.04 and 7.2 ks. Also, Table 3 includes the measured values of the yield strength (YS), ultimate tensile strength (UTS) and fracture strain for the various specimens. The UTS and fracture strain in the ST specimen were ~830 MPa and ~16.4%, respectively, while after HPT-processing the UTS was enhanced to ~2230 MPa with a related decrease in the fracture elongation to ~3.1%. After PDA for 0.04 ks, the UTS was decreased to ~1340 MPa and the strain to fracture increased around four times to ~11.9% due to the formation of the reversed austenite in the microstructure and the reduction in the dislocations density by a recovery process. Finally, PDA for 7.2 ks led to a reduction in the UTS to ~975 MPa and an increase in the fracture strain to ~14.4%.

The fracture surfaces of the initial ST specimen, HPT-processed sample and the PDA-processed specimens for 0.04 and 7.2 ks after tensile testing are presented in Fig. 8. It is

Table 2 – Average grain size of the martensite and austenite phases achieved from the EBSD results in different conditions.

Condition	α′-martensite (nm)	γ-austenite (nm)
ST	~ 5200	–
HPT	~ 185	~ 28
PDA (0.04 ks)	~ 195	~ 180
PDA (0.48 ks)	~ 360	~ 245
PDA (1.8 ks)	~ 540	~ 270
PDA (7.2 ks)	~ 570	~ 280

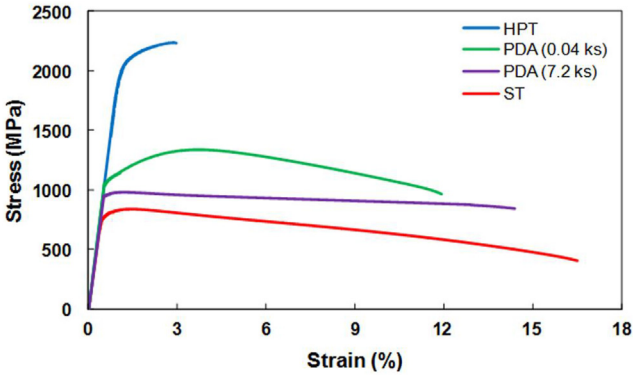

Fig. 7 – Engineering stress-engineering strain curves for the ST specimen, the HPT-processed sample, and the PDA-processed specimens for 0.04 and 7.2 ks.

Table 3 – Yield strength (YS), ultimate tensile strength (UTS) and fracture strain values for specimens in various conditions.

Condition	YS (MPa)	UTS (MPa)	Fracture Strain (%)
ST	790	830	16.4
HPT	2040	2230	3.1
PDA (0.04 ks)	1050	1340	11.9
PDA (7.2 ks)	940	975	14.4

obvious that there are considerable differences in the fractography of specimens in different conditions. In the ST specimen (Fig. 8(a)), the surface indicates a ductile fracture manner due to the presence of the dimple morphology with various sizes and depths. After HPT processing (Fig. 8(b)), there is a combination of fine dimples and cave-like shear band cracks in the fracture surface suggesting a mixture of ductile and brittle fracture modes. For the PDA-processed specimens for 0.04 and 7.2 ks (Fig. 8(c) and (d)), the fracture surfaces display again dimples with smaller sizes than for the ST specimen which prove the appearance of a ductile fracture mode.

4. Discussion

4.1. *Microstructure and phase evolution*

From the EBSD results in Fig. 4, it is apparent that the ST specimen has a lath α'-martensite microstructure with a high amount of LAGBs related to the high density of dislocations (Fig. 4(a)). It is well known that the lath martensitic structure consists of martensite lath, block, and packet [39]. As a simple rule, martensite lath is a single crystal of martensite having large numbers of dislocations and lattice defects. The block is also known as martensite variant that is the laths with the same crystallographic orientation. The packet consists of blocks having the same plane of parent austenite [40]. The HPT processing leads to the transformation of a considerable portion of the LAGBs to HAGBs and creates a mixture of equiaxed and elongated grains of martensite oriented along the shear strain direction (Fig. 4(b)). This is in good agreement with the conventional trends related to the microstructural evolution in metals and alloys processed by SPD techniques [41]. During the SPD processing of the lath martensitic steel, the microstructure is severely distorted and the substructure of lath martensite (blocks or packets) is suppressed. In this case, a number of dislocations are introduced and they pile up and eventually form new low-angle boundaries. By increasing the strain, the low-angle boundaries are transformed to high-angle grain boundaries and therefore, the equiaxed and refined grains of martensite are formed [42,43]. Furthermore, it is obvious that the HPT processing creates a low amount of the fine-grained austenite in the initial martensitic matrix due to the strain accumulation and the resultant boost in temperature which is not detected by XRD. This is likely due to the low amount of austenite and its very small grain size. Earlier reports described the possibility of austenite formation as a consequence of a strain-induced reverse transformation in SPD processing if the applied stress on the material supplied the necessary driving force for the reverse transformation [4,5,44]. Under HPT, a large fraction of the mechanical work

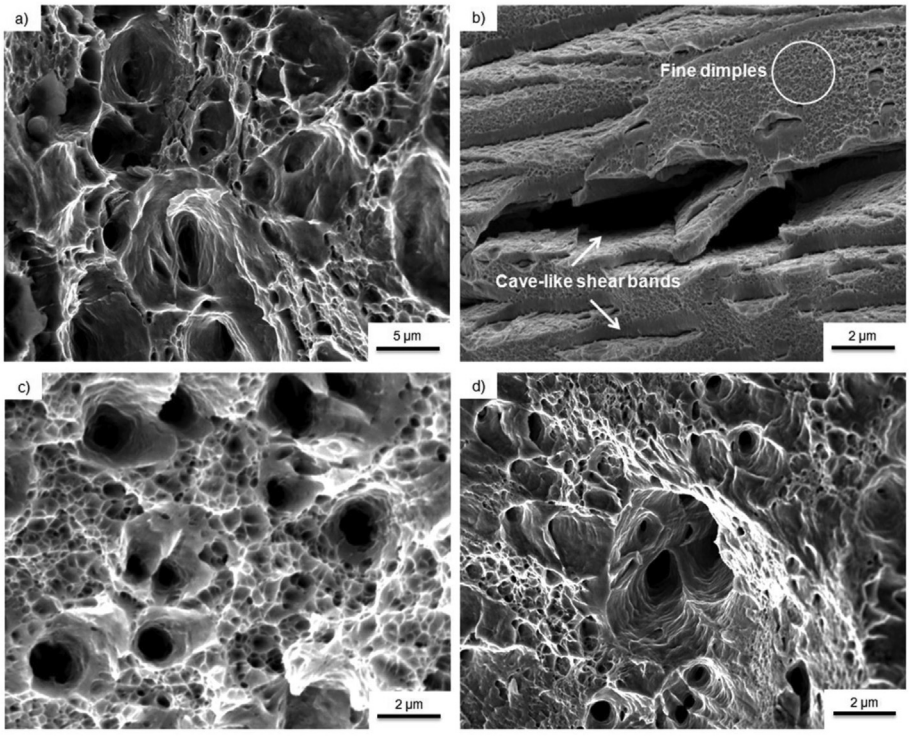

Fig. 8 – FE-SEM micrographs of fracture surfaces of (a) the ST specimen, (b) the HPT-processed sample, and the PDA-processed specimens for (c) 0.04 ks and (d) 7.2 ks.

converts to heat which leads to an increase in the specimen temperature [45]. Also, based on the Clausius–Clapeyron relationship, the imposed pressure on the material results in a significant decrease in the equilibrium temperature of the phase transformation [46].

From another point of view, the martensite with a lath morphology includes a high density of dislocations and under the reverse transformation the dislocations energy is released to some degree as a consequence of the reversed austenite formation. In fact, it is well-known that these different parameters lead to a decrease in the necessary driving force and enhance the occurrence of the strain-induced reverse transformation [4]. Additionally, the EBSD micrographs in Fig. 4(c)–(f) show that during PDA of the HPT-processed specimens a large fraction of the fine and coaxial grains of austenite nucleates in the deformed martensitic microstructure after only 0.04 ks (Fig. 4(c)) so that its volume fraction drastically decreases by increasing the annealing time (Fig. 4(d)–(f)). The austenite formation under this condition is related to the occurrence of a reverse transformation through PDA. In addition, as indicated in Fig. 4(c)–(f) and Table 2, it is apparent that, with an increase in the annealing time from 0.04 to 7.2 ks, the average grain size of the retained austenite was increased from about 180 nm to around 280 nm, respectively, due to the grain growth phenomena. It was reported that the austenite stability is affected by different parameters including the grain size, re-crystallization and the orientation gradient of austenite [47]. Increasing the annealing time causes an increase in the grain size of austenite and consequently raises the start temperature of martensite formation (M_s) [48]. Therefore, the austenite stability can be reduced with an increase in annealing time.

As illustrated in Fig. 3, the calculated amount of the retained austenite at ambient temperature using data of Fig. 2 reveals that the retained austenite value in the PDA-processed specimen for 0.04 ks is about 58% which decreases significantly to only about 6% after 7.2 ks annealing time. It has been shown that the maximum austenite content of the homogenized specimen after annealing at 600 °C for 7.2 ks is around 40% which is lower than the austenite content of the short time PDA in this study [13]. The presence of nano-grained austenite which stimulates further austenite nucleation, together with nano-grained martensite including a high dislocation density which suppresses the M_s temperature, appears to enhance the kinetics and volume fraction of the reverse transformation.

The abrupt formation of a large amount of the reversed austenite in the initial annealing times and its instability at later stages of reversion indicates that the reverse transformation probably occurs by a diffusionless shear mechanism. It has been well clarified that a diffusionless shear transformation is described with a fast change in the atomic array that does not depend on time but it depends only on the reversion temperature [49]. An earlier report suggested that the reversed austenite formation under annealing of the solution-treated Fe-9.6Ni-7.1Mn (at.%) steel at 600 °C for 7.2 ks was taking place with a consecutive mixture of two mechanisms, consisting of diffusionless shear and diffusional mechanisms, as the volume fractions of the reversed austenite formed by each of these mechanisms were measured at about 40% and 18%, respectively [17]. By contrast, in the present research all of the 58% reversed austenite was formed by a diffusionless shear mechanism in the initial times of PDA and there was no driving force for activating the diffusional mechanism. This is attributed to the effects of post-HPT processing on the starting material such as the strain concentration, grain refinement and strain-induced austenite formation. In addition, it seems that the volume fraction of the reversed austenite during PDA at 600 °C is almost constant for different annealing times before water cooling to room temperature.

4.2. *Mechanical properties*

According to the microhardness measurements for the HPT-processed sample and the PDA-processed specimens for different annealing times in Fig. 6, and also investigating the EBSD maps in Fig. 4, it is anticipated that the high hardness value of the HPT-processed sample (690 Hv) is related to the very high concentration of dislocations in the material and the grain refinement of the microstructure. After PDA for only 0.04 ks, the hardness value decreases significantly to about 445 Hv due to dislocation annihilation by a recovery process. Thereafter, further annealing leads to a re-transformation of the shear-formed austenite to new martensite having a ductile nature as well as grain growth of the microstructure resulting in a decline in the value of hardness.

As shown in Fig. 7 and indicated in Table 3, the YS and UTS values in the ST specimen are almost the same together and there is only a slight strain hardening associated with the high number of dislocations in the α'-martensite, whereas the alloy gives an elongation of around 16.4% because of its relatively ductile nature. Processing by HPT enhances the UTS value of the ST specimen to ~2230 MPa and simultaneously decreases its elongation to ~3.1%. This higher strength and lower elongation in HPT-processed sample is attributed to grain refinement and the high density of dislocations and shear bands introduced in the material [7]. After the PDA for 0.04 ks, the UTS is decreased to ~1340 MPa and the fracture strain is enhanced by about four times to ~11.9% which is associated with the formation of the reversed austenite in the microstructure and the reduction in dislocation density by a recovery process. By contrast to the other specimens, the tensile test results of this specimen show a pre- and post-uniform deformation (necking) with a sharp UTS. This difference is attributed to the bi-modal microstructure of the specimen which includes a high volume fraction of ductile austenite and a high dislocation martensite. Finally, PDA for 7.2 ks leads to a greater reduction of the UTS to ~975 MPa and an increase of the fracture strain to ~14.4% which is attributed to the decrease in the amount of the shear-formed austenite and the increase in the grain size by increasing the annealing time. Accordingly, PDA at initial times leads to a good combination of high strength and good ductility for the studied steel.

The SEM images of the fracture surfaces in Fig. 8 confirm the results of the tensile test. The ductile fracture surface of the ST specimen is in agreement with the recorded elongation of around 16.4% (Fig. 8(a)). After applying HPT (Fig. 8(b)), the fracture behavior changes from necking to shearing and therefore the surface of fracture indicates a mixture of ductile

and brittle manner as reported earlier [9,50]. The presence of ultrafine dimples confirms the ductile fracture behavior of the sample [49,51] and the cave-like shear bands produced through shear deformation have a destructive effect on the evaluated elongation [52]. It is important to note that under the HPT processing, accumulation of deformation-induced vacancies produces small vacancy agglomerations. These agglomerates enlarge with increasing strain. During the tensile testing, shear bands form and generate progressively and the formation and propagation of these bands are revealed by the FE-SEM image from the fracture surfaces of specimens after HPT processing as shown in Fig. 8(b). As the shear bands have higher strains compared to the bulk material, more defects and correspondingly higher free energies are created in these regions [53]. This excess free energy supplies the required driving force for void formation during the shear deformation. As the shear deformation develops, if the local maximum shear stress exceeds the shear yield stress then the voids gradually transform to sub-micrometer or even microcracks [7] and these defects may reduce the overall ductility and affect the fracture behavior during tensile deformation. The fracture surfaces of the PDA-processed specimens for 0.04 and 7.2 ks (Fig. 8(c) and (d)) show again dimple shape morphology with smaller sizes by comparison with the ST specimen indicating a ductile facture mode with lower ductility.

5. Conclusions

This study evaluated the effects of HPT processing and PDA in the two phase (ferrite + austenite) region for different annealing times on the microstructure and mechanical behavior of a solution-treated Fe-9.6Ni-7.1Mn (at.%) steel with an initial martensitic microstructure. The investigation led to the following conclusions:

1. Processing by HPT led to the formation of a mixture of equiaxed and elongated martensitic ultrafine grains oriented along the shear strain direction accompanied by small amounts of the fine-grained austenite introduced by strain in the microstructure.
2. EBSD and XRD results confirmed that during PDA for 0.04 ks a large amount of fine and coaxial austenite grains was nucleated in the deformed microstructure by a diffusionless shear mechanism so that its volume fraction at ambient temperature was significantly reduced by increasing the annealing times.
3. After PDA for 7.2 ks, the average grain size was decreased from an initial value of about 5.2 μm in the solution-treated condition to ultrafine values of about 570 nm for the martensite and ~280 nm for the austenite.
4. The introduction of PDA produced an outstandingly good combination of the ultimate tensile strength (~1340 MPa) and fracture strain (~11.9%) in comparison to the initial solution-annealed condition. This is attributed to the finer grain size and the presence of shear-formed austenite in the microstructure.
5. The results obtained from tensile testing proved that the fracture mode changed from an entirely ductile nature in the solution-treated condition to a combination of ductile and brittle nature after HPT. The fracture surfaces of the PDA-processed specimens again showed ductile behavior.

Data availability

The raw/processed data required to reproduce these findings cannot be shared at this time as the data form part of an ongoing study.

Declaration of Competing Interest

The authors declare that they have no known competing financial interests or personal relationships that could have appeared to influence the work reported in this paper.

Acknowledgment

One of the authors was supported by the European Research Council under ERC Grant Agreement No. 267464-SPDMETALS (TGL).

REFERENCES

[1] Hossein Nedjad S, Nili-Ahmadabadi M, Furuhara T. Transmission electron microscopy study on the grain boundary precipitation of an Fe-Ni-Mn maraging steel. Metall Mater Trans A 2008;39:19–27. https://doi.org/10.1007/s11661-007-9407-z.

[2] Hossein Nedjad S, Nili Ahmadabadi M, Furuhara T, Maki T. High resolution transmission electron microscopy study on the nano-scale twinning of θ-NiMn precipitates in an Fe-Ni-Mn maraging alloy. Phys Status Solidi A 2006;203:2229–35. https://doi.org/10.1002/pssa.200566023.

[3] Hossein Nedjad S, Nili Ahmadabadi M, Furuhara T. Correlation between the intergranular brittleness and precipitation reactions during isothermal aging of an Fe-Ni-Mn maraging stee. Mater Sci Eng A 2008;490:105–12. https://doi.org/10.1016/j.msea.2008.01.070.

[4] Ghasemi-Nanesa H, Nili-Ahmadabadi M, Koohdar HR, Habibi-Parsa M, Hossein Nedjad S, Alidokht SA, et al. Strain-induced martensite to austenite reverse transformation in an ultrafine-grained Fe-Ni-Mn martensitic steel. Phil Mag 2014;94:1493–507. https://doi.org/10.1080/14786435.2014.886785.

[5] Koohdar HR, Nili Ahmadabadi M, Habibi-Parsa M, Ghasemi-Nanesa H. Investigating on the reverse transformation of martensite to austenite and pseudoelastic behavior in ultrafine-grained Fe-10Ni-7Mn (wt %) steel processed by heavy cold rolling. Adv Mater Res 2014;829:25–9. https://doi.org/10.4028/www.scientific.net/AMR.829.25.

[6] Koohdar HR, Nili Ahmadabadi M, Habibi-Parsa M, Jafarian HR, Ghasemi-Nanesa H, Shirazi H. Observation of pseudoelasticity in a cold rolled Fe-Ni-Mn martensitic steel. Mater Sci Eng A 2016;658:86–90. https://doi.org/10.1016/j.msea.2016.01.113.

[7] Mirsepasi A, Nili-Ahmadabadi M, Habibi-Parsa M, Ghasemi-Nanesa H, Dizaji AF. Microstructure and mechanical behavior of martensitic steel severely deformed by the novel

technique of repetitive corrugation and straightening by rolling. Mater Sci Eng A 2012;551:32–9. https://doi.org/10.1016/j.msea.2012.04.073.
[8] Shirazi H, Nili-Ahmadabadi M, Fatehi A, Hossein Nedjad S. Effect of severe plastic deformation on mechanical properties of Fe-Ni-Mn high strength steel. Adv Mater Res 2010;83:16–23. https://doi.org/10.4028/www.scientific.net/AMR.83-86.16.
[9] Kalahroudi FJ, Koohdar HR, Jafarian HR, Huang Y, Langdon TG, Nili-Ahmadabadi M. On the microstructure and mechanical properties of an Fe-10Ni-7Mn martensitic steel processed by high-pressure torsion. Mater Sci Eng A 2019;749:27–34. https://doi.org/10.1016/j.msea.2019.02.002.
[10] Kalahroudi FJ, Koohdar HR, Langdon TG, Nili-Ahmadabadi M. Phase evolution and mechanical properties of an intercritically-annealed Fe-10Ni-7Mn (wt. %) martensitic steel severely deformed by high-pressure torsion. Mater Sci Eng A 2021;804:140519. https://doi.org/10.1016/j.msea.2020.140519.
[11] Koohdar HR, Nili-Ahmadabadi M, Kalahroudi FJ, Jafarian HR, Langdon TG. The effect of high-pressure torsion on the microstructure and outstanding pseudoelasticity of a ternary Fe-Ni-Mn shape memory alloy. Mater Sci Eng A 2021;802:140647. https://doi.org/10.1016/j.msea.2020.140647.
[12] Iwabuchi Y. Toughness deterioration of 13Cr-3.8 Ni cast steel in the process of tempering. ISIJ Int 1984;70:701–8. https://doi.org/10.2355/tetsutohagane1955.70.7_701.
[13] Koohdar HR, Nili-Ahmadabadi M, Habibi-Parsa M, Jafarian HR. Development of pseudoelasticity in Fe-10Ni-7Mn (wt. %) high strength martensitic steel by intercritical heat treatment and subsequent ageing. Mater Sci Eng A 2015;621:52–60. https://doi.org/10.1016/j.msea.2014.10.049.
[14] Apple CA, Krauss G. The effect of heating rate on the martensite to austenite transformation in Fe-Ni-C alloys. Acta Metall 1972;20:849–56. https://doi.org/10.1016/0001-6160(72)90077-6.
[15] Jelenkowski J. Studies of the $\alpha' \rightarrow \gamma$ transformation in Fe-(23–26)Ni-2Ti alloys containing an addition of aluminium or molybdenum. J Mater Process Technol 1997;64:207–14. https://doi.org/10.1016/S0924-0136(96)02569-1.
[16] Lee SJ, Park Y, Lee YK. Reverse transformation mechanism of martensite to austenite in a metastable austenitic alloy. Mater Sci Eng A 2009;515:32–7. https://doi.org/10.1016/j.msea.2009.02.010.
[17] Koohdar HR, Nili Ahmadabadi M, Habibi-Parsa M, Jafarian HR, Bhattacharjee T, Tsuji N. On the stability of reversely formed austenite and related mechanism of transformation in an Fe-Ni-Mn martensitic steel aided by electron backscattering diffraction and atom probe tomography. Metall Mater Trans A 2017;48:5244–57. https://doi.org/10.1007/s11661-017-4288-2.
[18] Valiev RZ, Islamgaliev RK, Alexandrov IV. Bulk nanostructured materials from severe plastic deformation. Prog Mater Sci 2000;45:103–89. https://doi.org/10.1016/S0079-6425(99)00007-9.
[19] Valiev RZ, Estrin Y, Horita Z, Langdon TG, Zehetbauer MJ, Zhu YT. Fundamentals of superior properties in bulk NanoSPD materials. Mater Res Lett 2016;4:1–21. https://doi.org/10.1080/21663831.2015.1060543.
[20] Zhilyaev AP, Langdon TG. Using high-pressure torsion for metal processing: fundamentals and applications. Prog Mater Sci 2008;53:893–979. https://doi.org/10.1016/j.pmatsci.2008.03.002.
[21] Huang Y, Figueiredo RB, Baudin T, Brisset F, Langdon TG. Evolution of strength and homogeneity in a magnesium AZ31 alloy processed by high-pressure torsion at different temperatures. Adv Eng Mater 2012;14:1018–26. https://doi.org/10.1002/adem.201200016.
[22] Shi S, Zhang Z, Wang X, Zhou G, Xie G, Wang D, et al. Microstructure evolution and enhanced mechanical properties in SUS316LN steel processed by high pressure torsion at room temperature. Mater Sci Eng A 2018;711:476–83. https://doi.org/10.1016/j.msea.2017.11.064.
[23] Gubicza J, El-Tahawy M, Huang Y, Choi H, Choe H, Lábár JL, et al. Microstructure, phase composition and hardness evolution in 316L stainless steel processed by high-pressure torsion. Mater Sci Eng A 2016;657:215–23. https://doi.org/10.1016/j.msea.2016.01.057.
[24] An XH, Lin QY, Sha G, Huang MX, Ringer SP, Zhu YT, et al. Microstructural evolution and phase transformation in twinning-induced plasticity steel induced by high-pressure torsion. Acta Mater 2016;109:300–13. https://doi.org/10.1016/j.actamat.2016.02.045.
[25] Čižek J, Janeček M, Vlasák T, Smola B, Melikhova O, Islamgaliev RK, et al. The development of vacancies during severe plastic deformation. Mater Trans 2019;60:1533–42. https://doi.org/10.2320/matertrans.MF201937.
[26] Muller T, Kapp MW, Bachmaier A, Felfer P, Pippan R. Ultrahigh-strength low carbon steel obtained from the martensitic state via high pressure torsion. Acta Mater 2019;166:168–77. https://doi.org/10.1016/j.actamat.2018.12.028.
[27] Xu C, Dobatkin SV, Horita Z, Langdon TG. Superplastic flow in a nanostructured aluminum alloy produced using high-pressure torsion. Mater Sci Eng A 2009;500:170–5. https://doi.org/10.1016/j.msea.2008.09.049.
[28] Muller T, Bachmaier A, Stark A, Schell N, Pippan R. Nanostructured low carbon steels obtained from the martensitic state via severe plastic deformation, precipitation, recovery, and recrystallization. Adv Eng Mater 2019;21:1800202. https://doi.org/10.1002/adem.201800202.
[29] El-Tahawy M, Huang Y, Choi H, Choe H, Lábár JL, Langdon TG, et al. High temperature thermal stability of nanocrystalline 316L stainless steel processed by high-pressure torsion. Mater Sci Eng A 2017;682:323–31. https://doi.org/10.1016/j.msea.2016.11.066.
[30] Shen YF, Jia N, Wang YD, Sun X, Zuo L, Raabe D. Suppression of twinning and phase transformation in an ultrafine grained 2GPa strong metastable austenitic steel: experiment and simulation. Acta Mater 2015;97:305–15. https://doi.org/10.1016/j.actamat.2015.06.053.
[31] Chen S, Shibata A, Zhao LJ, Gao S, Tian YZ, Tsuji N. Microstructural evolution of metastable austenitic steel during high-pressure torsion and subsequent heat treatment. IOP Conf Ser: Mater Sci Eng 2014;63:012053.
[32] El-Tahawy M, Pereira PHR, Huang Y, Park H, Choe H, Langdon TG, et al. Exceptionally high strength and good ductility in an ultrafine-grained 316L steel processed by severe plastic deformation and subsequent annealing. Mater Lett 2018;214:240–2. https://doi.org/10.1016/j.matlet.2017.12.040.
[33] Takaki S, Tomimura K, Ueda S. Effect of pre-cold-working on diffusional reversion of deformation induced martensite in metastable austenitic stainless steel. ISIJ Int 1994;34:522–7. https://doi.org/10.2355/isijinternational.34.522.
[34] Misra RDK, Nayak S, Venkatasurya PKC, Ramuni V, Somani MC, Karjalainen LP. Nanograined/ultrafine-grained structure and tensile deformation behavior of shear phase reversion-induced 301 austenitic stainless steel. Metall Mater Trans 2010;41:2162–74. https://doi.org/10.1007/s11661-010-0230-6.
[35] Rajasekhara S, Karjalainen LP, Kyröläinen A, Ferreira PJ. Microstructure evolution in nano/submicron grained AISI 301LN stainless steel. Mater Sci Eng A 2010;527:1986–96. https://doi.org/10.1016/j.msea.2009.11.037.

[36] Herrera C, Plaut RL, Padilha AF. Microstructural refinement during annealing of plastically deformed austenitic stainless steels. Mater Sci Forum 2007;550:423–8. https://doi.org/10.4028/www.scientific.net/MSF.550.423.
[37] Almathami A, Goodall G, Brochu M. Crystal structure, transformation and thermal stability of nanostructured 316LSS alloyed with 2 and 6 wt.% aluminum. Mater Sci Eng A 2010;527:6020–7. https://doi.org/10.1016/j.msea.2010.06.001.
[38] Figueiredo RB, Pereira PHR, Aguilar MTP, Cetlin PR, Langdon TG. Using finite element modeling to examine the temperature distribution in quasi-constrained high-pressure torsion. Acta Mater 2012;60:3190–8. https://doi.org/10.1016/j.actamat.2012.02.027.
[39] Krauss G. Steels: heat treatment and processing principles. Ohio: ASM Int.; 1990.
[40] Kitahara H, Ueji R, Tsuji N, Minamino Y. Crystallographic features of lath martensite in low-carbon steel. Acta Mater 2006;54:1279–88. https://doi.org/10.1016/j.actamat.2005.11.001.
[41] Cao Y, Ni S, Liao X, Song M, Zhu Y. Structural evolutions of metallic materials processed by severe plastic deformation. Mater Sci Eng R: Rep 2018;133:1–59. https://doi.org/10.1016/j.mser.2018.06.001.
[42] Jafarian HR, Tarazkouhi MF. Significant enhancement of tensile properties through combination of severe plastic deformation and reverse transformation in an ultrafine/nano grain lath martensitic steel. Mater Sci Eng A 2017;686:113–20. https://doi.org/10.1016/j.msea.2017.01.034.
[43] Fan ZQ, Hao T, Zhao SX, Luo GN, Liu CS, Fang QF. The microstructure and mechanical properties of T91 steel processed by ECAP at room temperature. J Nucl Mater 2013;434:417–21. https://doi.org/10.1016/j.jnucmat.2012.12.009.
[44] Ghasemi-Nanesa H, Nili Ahmadabadi M, Shirazi H, Hossein Nedjad S. Observation of reverse transformation of α-ε-γ in ultrafine-grained Fe-Ni-Mn age hardenable martensitic steel. Int J Mod Phys: Conf Ser 2012;5:9–17. https://doi.org/10.1142/S201019451200178X.
[45] Edalati K, Hashiguchi Y, Pereira PHR, Horita Z, Langdon TG. Effect of temperature rise on microstructural evolution during high-pressure torsion. Mater Sci Eng A 2018;714:167–71. https://doi.org/10.1016/j.msea.2017.12.095.
[46] Ivanisenko Y, Maclaren I, Sauvage X, Valiev R, Fecht H. Shear-induced α→γ transformation in nanoscale Fe-C composite. Acta Mater 2006;54(6):1659–69. https://doi.org/10.1016/j.actamat.2005.11.034.
[47] Wang HZ, Yang P, Mao WM, Lu FY. Effect of hot deformation of austenite on martensitic transformation in high manganese steel. J Alloys Compd 2013;558:26–33. https://doi.org/10.1016/j.jallcom.2012.12.032.
[48] Yang HS, Bhadeshia HKDH. Austenite grain size and the martensite start temperature. Scripta Mater 2009;60:493–5. https://doi.org/10.1016/j.scriptamat.2008.11.043.
[49] Nishiyama Z. Martensitic transformation. New York: Academic Press; 1978.
[50] Karavaeva MV, Kiseleva SK, Abramova MM, Ganeev AV, Valiev RZ. Microstructure, properties, and failure characteristics of medium-carbon steel subjected to severe plastic deformation. IOP Conf Ser: Mater Sci Eng 2014;63:012056. https://doi.org/10.1088/1757-899x/63/1/012056.
[51] Hohenwarter A, Taylor A, Stock R, Pippan R. Effect of large shear deformations on the fracture Behavior of a fully pearlitic steel. Metall Mater Trans 2010;42:1609–18. https://doi.org/10.1007/s11661-010-0541-7.
[52] Ruffing C, Kobler A, Courtois-Manara E, Prang R, Kübel C, Ivanisenko Y, et al. Fatigue behavior of ultrafine-grained medium carbon steel with different carbide morphologies processed by high pressure torsion. Metals 2015;5:891–909. https://doi.org/10.3390/met5020891.
[53] Tian YZ, Li JJ, Zhang P, Wu SD, Zhang ZF, Kawasaki M, et al. Microstructures, strengthening mechanisms and fracture behavior of Cu-Ag alloys processed by high-pressure torsion. Acta Mater 2012;60(1):269–81. https://doi.org/10.1016/j.actamat.2011.09.058.